

Supporting Information

Fine-tuning of nano-traps in a stable metal–organic framework for highly efficient removal of propyne from propylene

Hui-Min Wen,^{‡a,b} Libo Li,^{‡b} Rui-Biao Lin,^b Bin Li,^{*c} Bin Hu,^d Wei Zhou,^e Jun Hu^{*a} and Banglin Chen^{*b}

^a College of Chemical Engineering, Zhejiang University of Technology, Zhejiang, 310014, P. R. China. E-mail: hjzjut@zjut.edu.cn

^b Department of Chemistry, University of Texas at San Antonio, One UTSA Circle, San Antonio, Texas 78249-0698, USA. Fax: (+1)-210-458-7428. E-mail: banglin.chen@utsa.edu

^c State Key Laboratory of Silicon Materials, Cyrus Tang Center for Sensor Materials and Applications, School of Materials Science and Engineering, Zhejiang University, Hangzhou, 310027. E-mail: bin.li@zju.edu.cn

^d Key Laboratory of Jiangxi Province for Persistent Pollutants Control and Resources Recycle, School of Environmental and Chemical Engineering, Nanchang Hangkong University, Nanchang 330063, China

^e NIST Center for Neutron Research, National Institute of Standards and Technology, Gaithersburg, MD 20899-6102, USA

[‡] These authors have contributed equally to this work.

1. Powder X-ray Crystallography. Attempts to obtain single crystals for single-crystal X-ray diffraction measurement were not successful. We thus relied on powder X-ray diffraction (PXRD) to confirm the high purity of the powder sample and to simulate the crystallographic structure.^[1] The samples were sealed in glass capillaries, and PXRD measurements were performed on a Rigaku Ultima IV diffractometer, operated at 40 kV and 44 mA and CuK α radiation ($\lambda = 1.5406 \text{ \AA}$). Data were collected at room temperature in the 2θ range of $2\text{--}45^\circ$ with a step size of 0.5° .

We first indexed the PXRD pattern and identified a monoclinic $B2$ space group. Here we chose the $B2$ setting, instead of the standard $C2$ setting, in order to build an ordered structure in a less oblique unit cell and to show the channel pore structure more clearly (*i.e.*, the channel pore would be along the crystallographic c axis under the $B2$ setting). Then, based on the framework connection of SIFSIX-3-Ni, we built a crystal structure model for ZJUT-1. The -NH_2 groups were modeled as fully ordered in the structure. In reality, there might exist some orientational disorder associated with the -NH_2 groups. Unit cell parameters of ZJUT-1 are $a = c = 9.9363(1) \text{ \AA}$, $b = 7.5660(1) \text{ \AA}$, and $\alpha = \beta = \gamma = 90.00$ (Table S1). The slightly larger lengths of the a - and c -axes in the unit cell parameters of ZJUT-1 compared with SIFSIX-3-Ni (7.0148 \AA) are mainly attributed to the incorporation of amino groups.^[2,3]

2. Virial Graph Analysis

Estimation of the isosteric heats of gas adsorption (Q_{st})

A virial-type expression of comprising the temperature-independent parameters a_i and b_j was employed to calculate the enthalpies of adsorption for C_3H_4 (at 273 K and 298 K) on ZJUT-1a. In each case, the data were fitted use equation:

$$\ln P = \ln N + 1/T \sum_{i=0}^m a_i N_i + \sum_{j=0}^n b_j N_j \quad (1)$$

Here, P is the pressure expressed in Pa, N is the amount absorbed in mmol g^{-1} , T is the temperature in K, a_i and b_j are virial coefficients, and m , n represent the number of coefficients required to adequately describe the isotherms (m and n were gradually increased till the contribution of extra added a and b coefficients was deemed to be statistically insignificant towards the overall fit. And the average value of the squared deviations from the experimental values was minimized). The

values of the virial coefficients a_0 through a_m were then used to calculate the isosteric heat of absorption using the following expression:

$$Q_{st} = -R \sum_{i=0}^m a_i N_i \quad (2)$$

Q_{st} is the coverage-dependent isosteric heat of adsorption and R is the universal gas constant. The heat enthalpy of C_3H_4 sorption for complex ZJUT-1a in this manuscript are determined by using the sorption data measured in the pressure range from 0-1 bar (at 273 K and 298 K).

3. IAST calculations of adsorption selectivities

The selectivity of preferential adsorption of component 1 over component 2 in a mixture containing 1 and 2, can be formally defined as:

$$S_{ads} = \frac{q_1/q_2}{p_1/p_2} \quad (3)$$

In equation (3), q_1 and q_2 are the absolute component loadings of the adsorbed phase in the mixture. These component loadings are also termed the uptake capacities. We calculate the values of q_1 and q_2 using the Ideal Adsorbed Solution Theory (IAST) of Myers and Prausnitz.

4. Fitting of pure component isotherms

Experimental data on pure component isotherms for C_3H_4 in ZJUT-1a were measured at 298 and 273 K. The pure component isotherm data for C_3H_4 and C_3H_6 were fitted with the Dual site Langmuir-Freundlich (DSLFF) model:

$$N = N_1^{max} \frac{b_1 p^{1/n_1}}{1 + b_1 p^{1/n_1}} + N_2^{max} \frac{b_2 p^{1/n_2}}{1 + b_2 p^{1/n_2}} \quad (4)$$

where p (unit: Kpa) is the pressure of the bulk gas at equilibrium with the adsorbed phase, N (unit: mol/Kg) is the adsorbed amount per mass of adsorbent, N_1^{max} and N_2^{max} (unit: mol/Kg) are the saturation capacities of sites 1 and 2, b_1 and b_2 (unit: 1/kPa) are the affinity coefficients of sites 1 and 2, and n_1 and n_2 represent the deviations from an ideal homogeneous surface. Here, the single-component C_3H_4 and C_3H_6 adsorption isotherms have been fit to enable the application of IAST in

simulating the performance of ZJUT-1a under a mixed component gas. Adsorption isotherms and gas selectivity calculated by IAST for 1/99 and 50/50 C₃H₄/C₃H₆ (v/v) mixtures in the ZJUT-1a.

5. GCMC simulations

All the GCMC simulations were performed in the MS modeling 5.0 package.⁴ The crystal structure of C₃H₄-loaded sample was chosen for related simulations without further geometry optimization. The framework and the individual C₃H₄ molecules were considered to be rigid during the simulation. Partial charges for atoms of guest-free ZJUT-1 were derived from QEq method and QEq_neutral1.0 parameter. The simulations were carried out at 298 K, adopting the locate task, Metropolis method in Sorption module and the universal force field (UFF). The partial charges on the atoms of C₃H₄ (C1: -0.125e, C2: 0.004e, C3: -0.39e; H1: 0.113e, H2: 0.133e, where e = 1.6022 × 10⁻¹⁹ C is the elementary charge) were also derived from QEq method. The interaction energy between hydrocarbon molecules and framework were computed through the Coulomb and Lennard-Jones 6-12 (LJ) potentials. The cutoff radius was chosen as 12.5 Å for the LJ potential and the long-range electrostatic interactions were handled using the Ewald & Group summation method. The loading steps and the equilibration steps were 1 × 10⁵, the production steps were 1 × 10⁶.

6. Stability tests

Powder samples of ZJUT-1 were exposed to the moisture with the humidity from 20% to 85% at 30 °C for 1d, respectively. This condition was achieved by using a constant temperature&humidity incubator. After the exposure, each sample were removed from the incubator and characterized by PXRD measurements in order to detect signs whether the sample have been affected by exposure to humidity or not. Studies on the exposure of ZJUT-1 to H₂S gas were also conducted under the N₂ flow (20 mL/min) containing 1% or 5% H₂S for 2 hours in order to test the stability of this material against acid gas. To further confirm the moisture stability of ZJUT-1, the sample was first exposed to the humidity of 80% for 1 day. After that, the sample was then activated to examine the C₃H₄ adsorption properties.

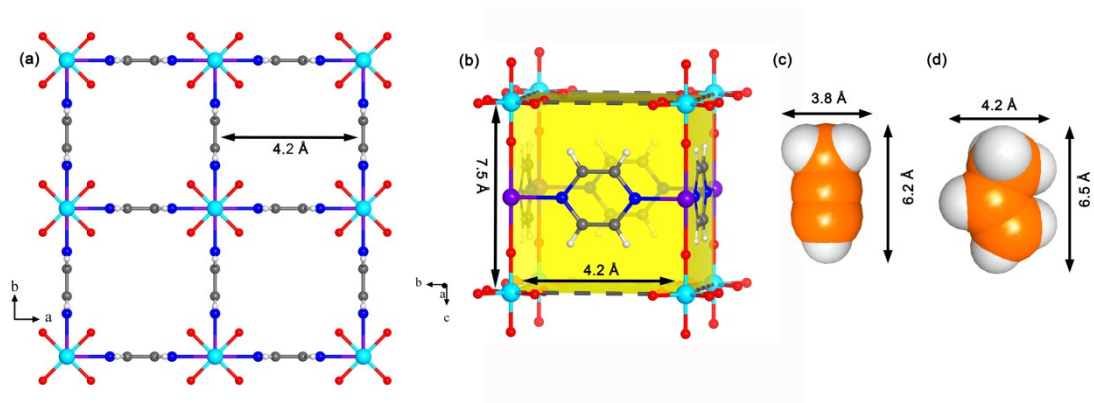


Figure S1. (a) Structure description of SIFSIX-3-Ni, highlighting its nanocages with the size of $7.5 \text{ \AA} \times 4.2 \text{ \AA} \times 4.2 \text{ \AA}$ that are separated by four SiF_6^{2-} anions. (c) The molecular size of C_3H_4 and C_3H_6 molecule (d).

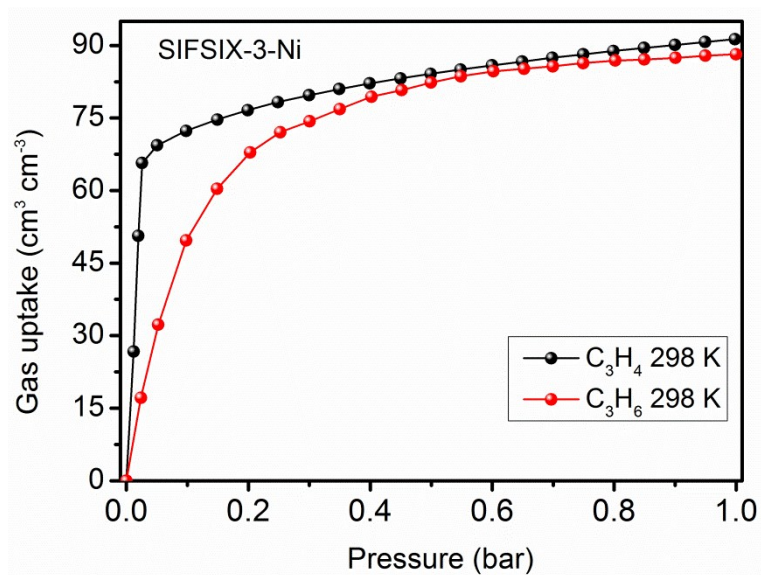


Figure S2. Adsorption isotherms of C_3H_4 (red) and C_3H_6 (black) for SIFSIX-3-Ni at 298 K and 1 bar, indicating that SIFSIX-3-Ni can adsorb large amount of both C_3H_4 and C_3H_6 gas.

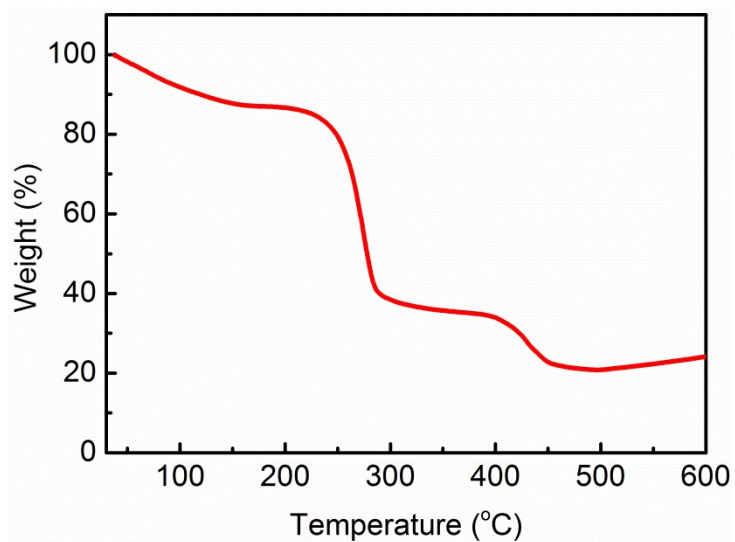


Figure S3. TGA curves of as-synthesized ZJUT-1.

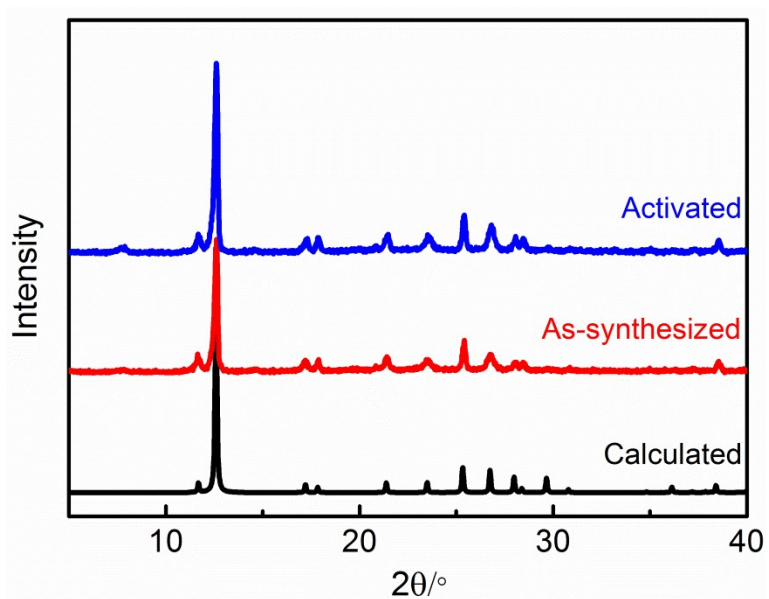


Figure S4. PXRD patterns of as-synthesized ZJUT-1 (red) and activated ZJUT-1 (blue) along with the calculated XRD pattern from the model structure of ZJUT-1 (black).

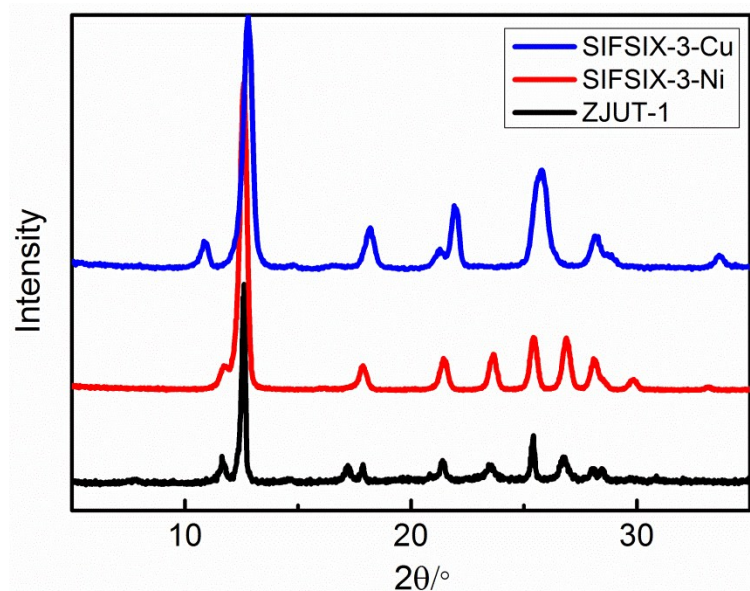


Figure S5. Experimental PXRD patterns of as-synthesized ZJUT-1, SIFSIX-3-Ni and SIFSIX-3-Cu, all of which match well with each other.

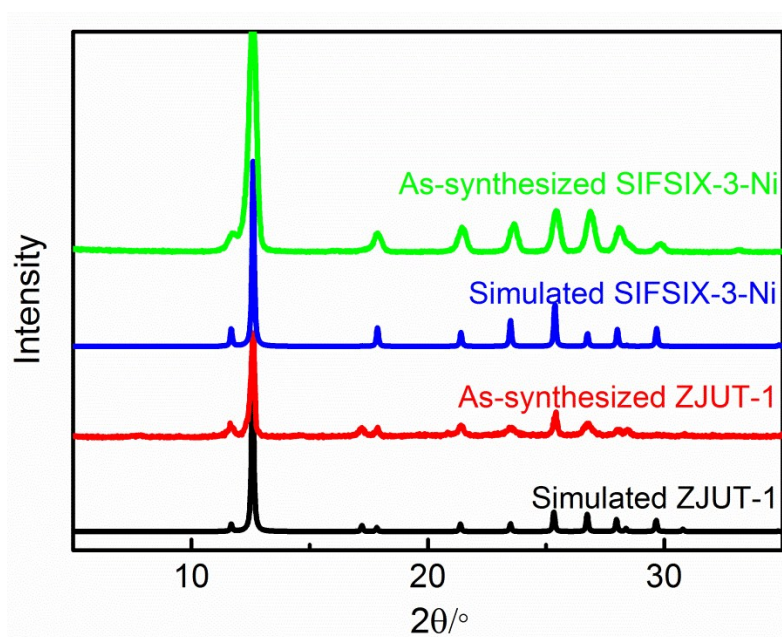


Figure S6. PXRD patterns of as-synthesized ZJUT-1 (red) and SIFSIX-3-Ni (green) compared with the calculated XRD pattern from the structure of ZJUT-1 (black) and SIFSIX-3-Ni (blue), strongly confirming that the structure of ZJUT-1 is isorecticular to the nets of SIFSIX-3-Ni.

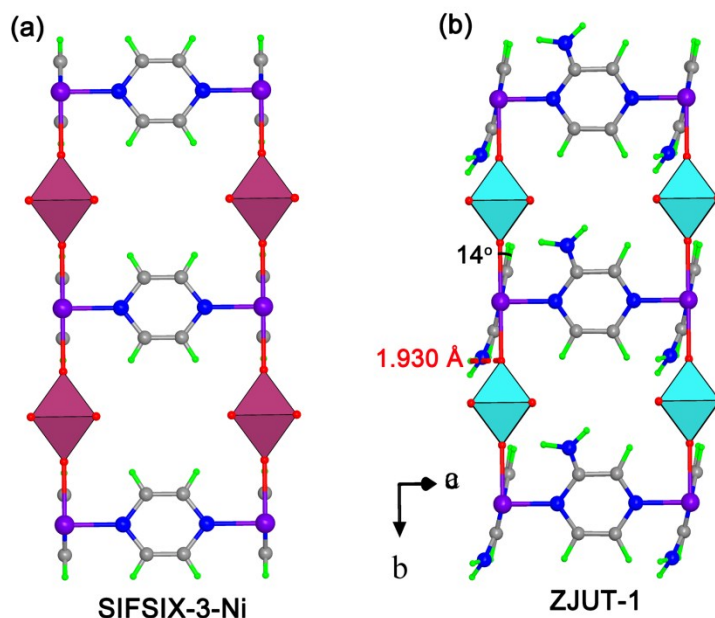


Figure S7. Structure comparison between SIFSIX-3-Ni and ZJUT-1 showing the impact of the use of a relatively bigger ligand (2-aminopyrazine) instead of pyrazine. (a) View of SIFSIX-3-Ni along *a*- and *b*-axes, showing the perfectly aligned pyrazine molecules. (b) View of ZJUT-1 along *a*- and *c*-axes, showing the titling of pyrazine molecules due to the use of the bigger ligand. This tilt of pyridine rings combined with the incorporation of amino groups thereby results in the aperture size being notably reduced from 4.2 Å in SIFSIX-3-Ni to 3.7 Å in ZJUT-1.

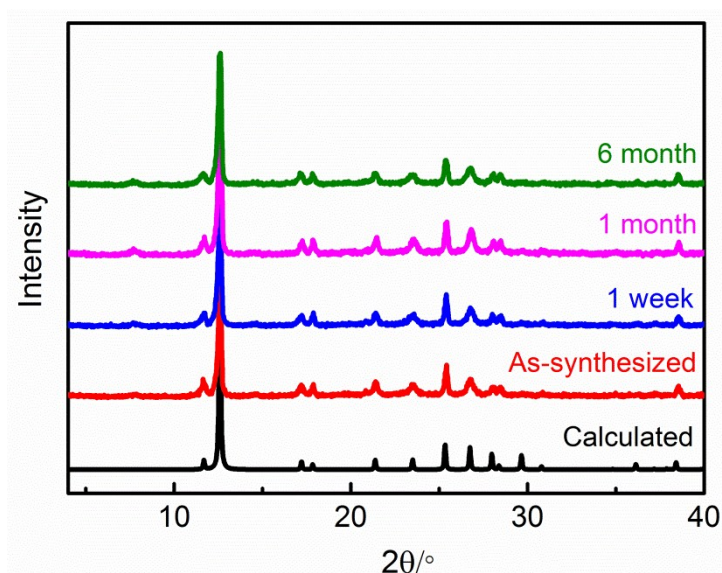


Figure S8. PXRD patterns of as-synthesized ZJUT-1 after exposed to air for more than 6 months.

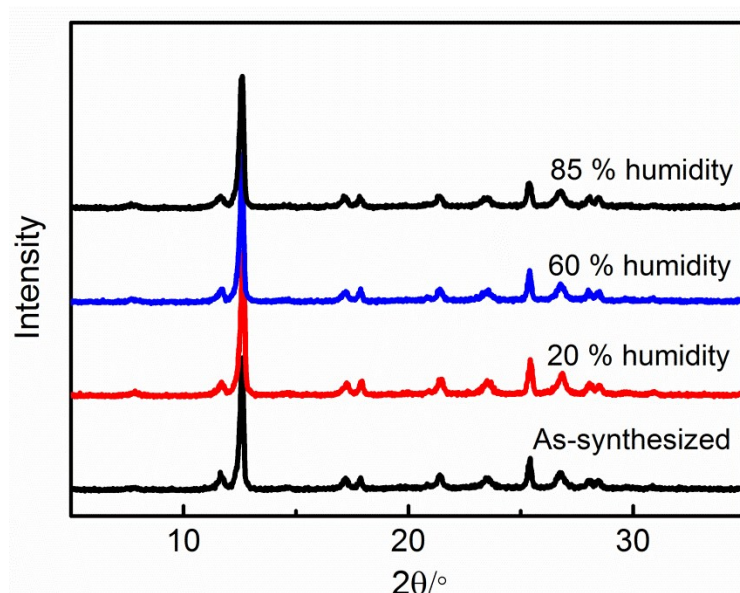


Figure S9. Experimental PXRD patterns of as-synthesized ZJUT-1 (red) and the sample exposed to variable humidity levels for one day.

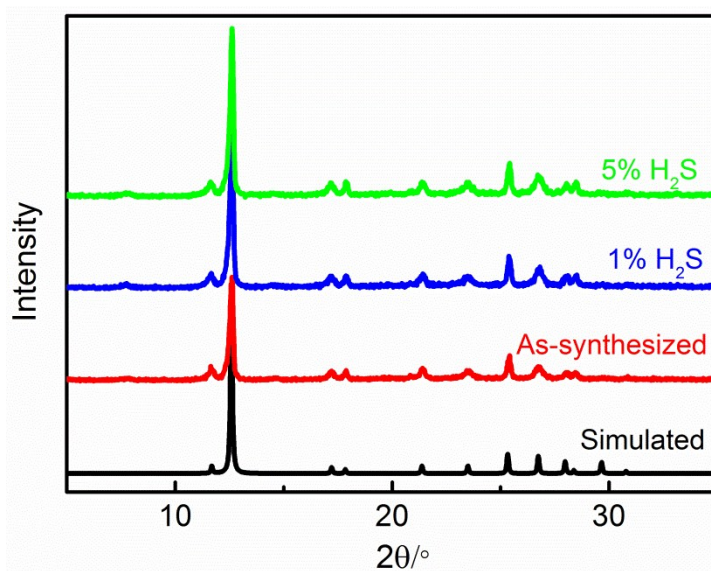


Figure S10. PXRD patterns of calculated (black), as-synthesized ZJUT-1 (red), and the sample exposed to variable H₂S concentrations (1% blue and 5% green) for one hour.

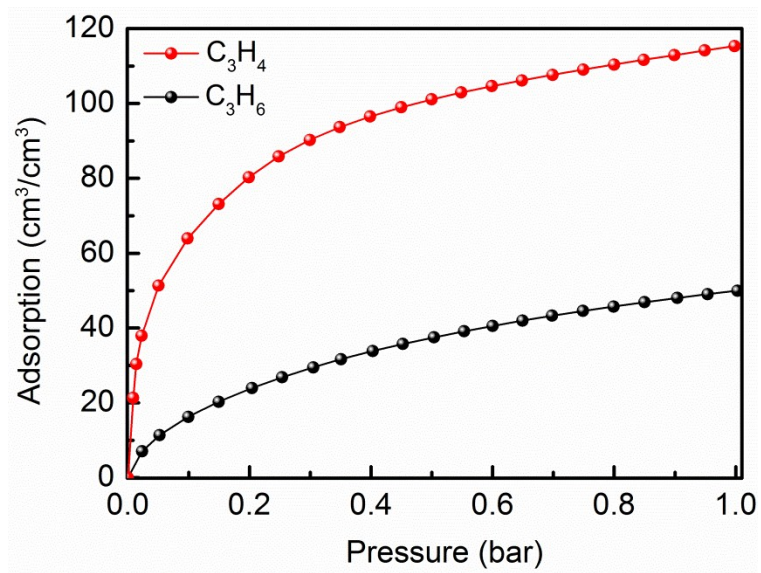


Figure S11. Adsorption isotherms of C_3H_4 (red) and C_3H_6 (black) for ZJUT-1a at 273 K up to 1bar.

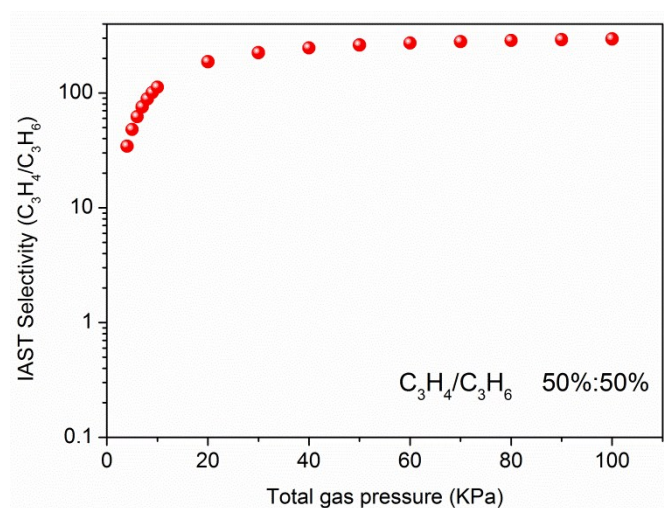


Figure S12. IAST selectivity of ZJUT-1a for C_3H_4/C_3H_6 (50/50, v/v) at 298 K.

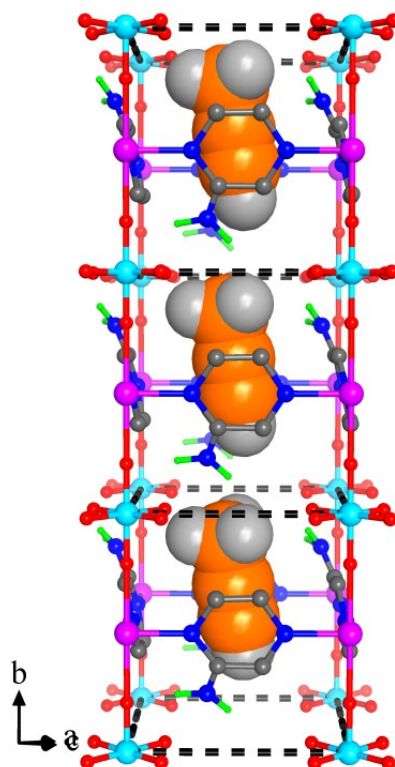


Figure S13. The calculated C_3H_4 adsorption binding sites in the nanocage of ZJUT-1a viewed along a - and c -axis, clearly indicating that one nanocage can only trap a single C_3H_4 molecule due to the suitable cage size, sharp, and functionalities.

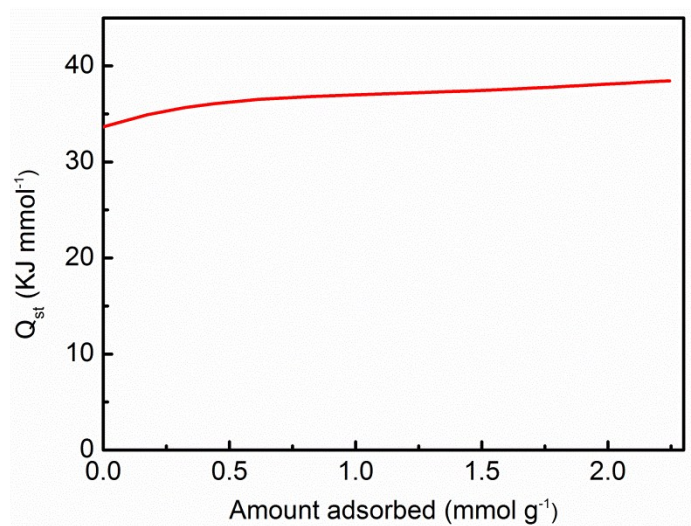


Figure S14. Heats of adsorption (Q_{st}) of C_3H_4 for ZJUT-1.

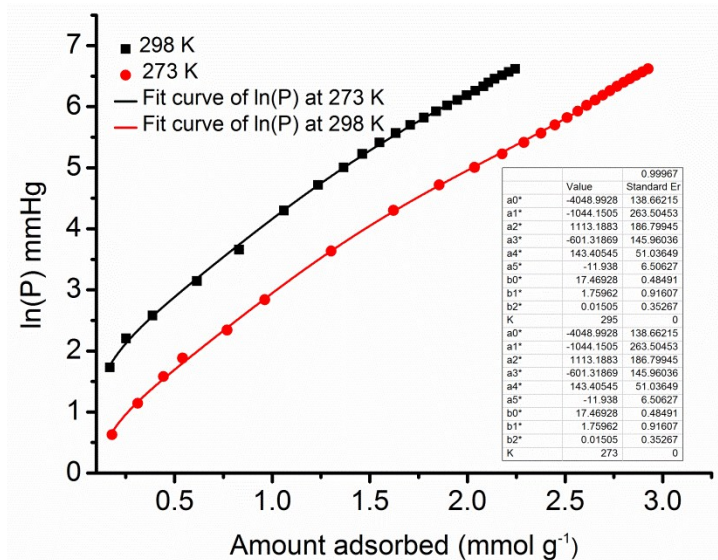


Figure S15. Virial fitting of the C_3H_4 adsorption isotherms for ZJUT-1.

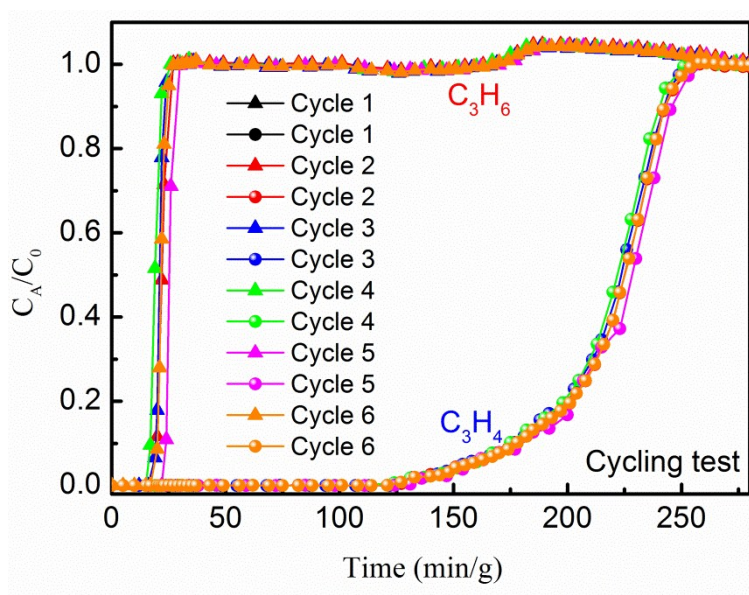


Figure S16. Cycling column breakthrough curves for C_3H_4/C_3H_6 separation (1/99, v/v) with ZJUT-1a at 298 K and 1.01 bar. The breakthrough experiments were carried out in a column packed with ZJUT-1a (Φ 4.0 \times 150 mm) at a flow rate of 2 ml/min.

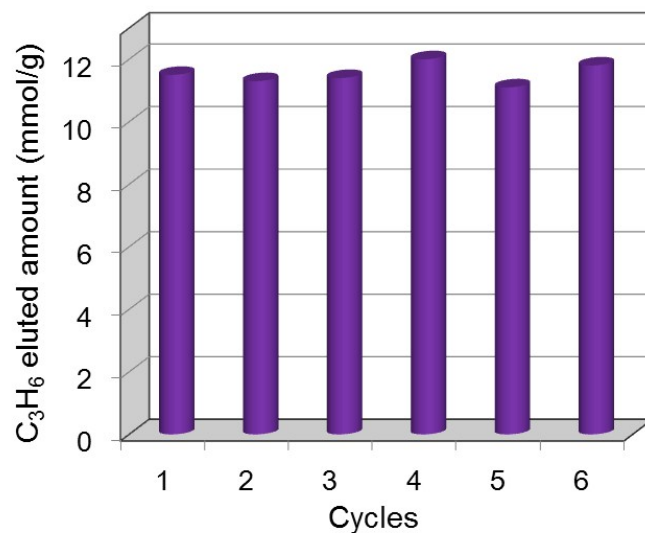


Figure S17. Cyclic breakthrough experiments on ZJUT-1a at 298 K and 1.01 bar, indicating that ZJUT-1a maintained the C₃H₆ eluted amount from the outlet effluent during the separation processes over at least 6 times.

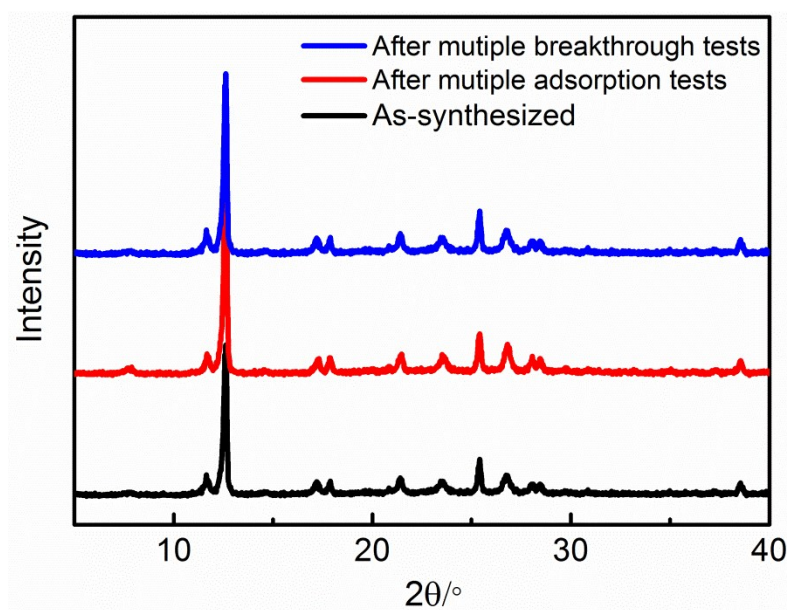


Figure S18. PXRD patterns of as-synthesized samples (black) and the samples after the multiple adsorption tests (red) and breakthrough tests (blue).

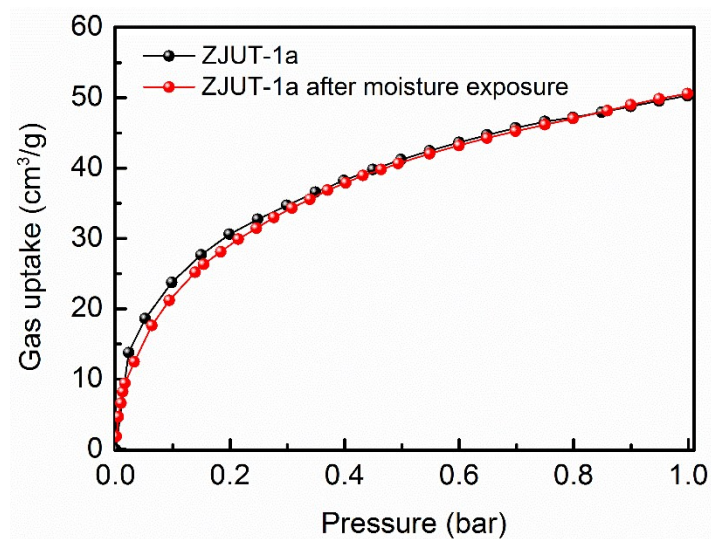
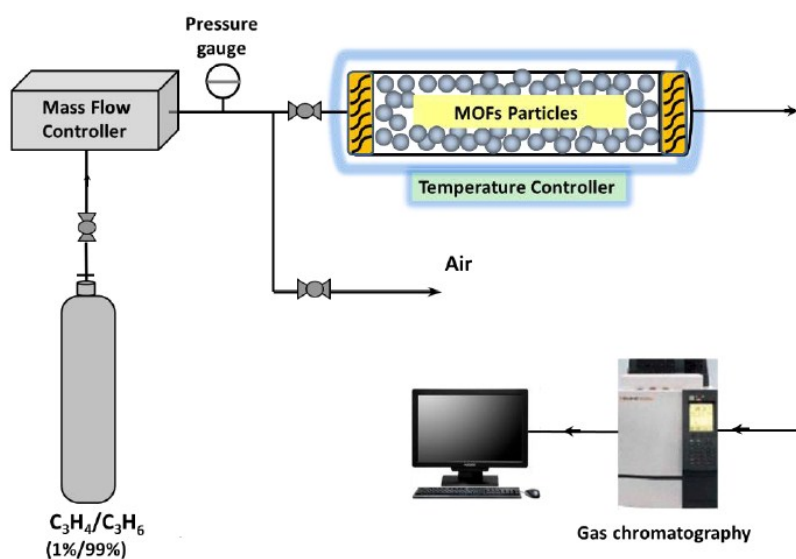


Figure S19. Comparison of C_3H_4 adsorption isotherms of ZJUT-1a (black) and the activated sample after the exposure to the humidity of 80% (red) for one day, confirming its good stability toward the moisture.



Breakthrough experiments apparatus

Figure S20. Schematic illustration of the apparatus for the breakthrough experiments.

Table S1. Lattice parameters of the modeled structure of ZJUT-1.

Unit cell parameters	ZJUT-1
Formula	C ₈ H ₁₀ NiF ₆ N ₆ Si
Formula weight	390.0
Crystal system	Monoclinic
Space group	<i>B2</i>
<i>a</i> , <i>c</i> (Å)	9.9363(1)
<i>b</i> (Å)	7.5660(1)
α (°)	90.00
β (°)	90.00
γ (°)	90.00
<i>V</i> (Å ³)	746.992
<i>Z</i>	2
<i>D</i> _{calcd} (g cm ⁻³)	1.738

Note: the -NH₂ groups were modeled as fully ordered in the structure. In reality, there might exist some orientational disorder associated with the -NH₂ groups.

Table S2. List of atomic coordinates for the modeled structure of ZJUT-1.

Atoms	x	y	z	s.o.f.
H1	0.30808	0.79196	0.02959	1.00
H2	0.19115	0.85914	0.14260	1.00
H3	0.36838	0.22857	0.19432	1.00
H4	0.12658	0.77250	0.30641	1.00
H5	0.18813	0.22091	0.35694	1.00
C6	0.27792	0.64293	0.18521	1.00
C7	0.31647	0.35149	0.21720	1.00
C8	0.17809	0.64474	0.28725	1.00
C9	0.21345	0.34782	0.31162	1.00
N10	0.27113	0.77465	0.12842	1.00
N11	0.35455	0.50000	0.14545	1.00
N12	0.14545	0.50000	0.35455	1.00
F13	0.33740	0.00000	0.00000	1.00
F14	0.50000	0.20810	0.00000	1.00
F15	0.50000	0.00000	-0.16260	1.00
F16	0.50000	0.00000	0.16260	1.00
Si17	0.50000	0.00000	0.00000	1.00
Ni18	0.50000	0.50000	0.00000	1.00

References

[1] G. Xu, B. Li, H. Wu, W. Zhou and B. Chen, *Cryst. Growth Des.*, **2017**, *17*, 4795–4800.

- [2] O. Shekhah, Y. Belmabkhout, K. Adil, P. M. Bhatt, A. J. Cairns and M. Eddaoudi, *Chem. Commun.*, **2015**, *51*, 13595–13598.
- [3] A. Kumar, D. G. Madden, M. Lusi, K.-J. Chen, E. A. Daniels, T. Curtin, J. J. Perry IV and M. J. Zaworotko, *Angew. Chem. Int. Ed.* **2015**, *54*, 14372 –14377.
- [4] *Accelrys*, Materials Studio Getting Started, release 5.0, Accelrys Software, Inc., San Diego, CA, **2009**.